1 **The immunomodulatory activity of extracellular vesicles derived**

2 **from endometrial mesenchymal stem cells on CD4+ T cells is**

3 **partially mediated by TGFbeta**

4 **Short title: The immunomodulation of EV-endMSCs is partially mediated by**

5 **TGFβ**

6 **Verónica Álvarez[1], Francisco Miguel Sánchez-Margallo[1,2], Beatriz Macías-García[3],**

7 **María Gómez-Serrano[2,4], Inmaculada Jorge[2,4], Jesús Vázquez[2,4], Rebeca Blázquez[1,2*],**

8 **Javier G Casado[1,2]**

9 [1]Stem Cell Therapy Unit, Jesus Uson Minimally Invasive Surgery Centre, Cáceres, Spain.

10 [2]CIBER de Enfermedades Cardiovasculares (CIBERCV), Madrid, Spain.

11 [3]Assisted Reproduction Unit, Jesus Uson Minimally Invasive Surgery Centre, Cáceres,

12 Spain.

13 [4] Centro Nacional de Investigaciones Cardiovasculares Carlos III (CNIC), Madrid, Spain.

14 *** Correspondence:**

15 Rebeca Blázquez. Stem Cell Therapy Unit, Jesus Usón Minimally Invasive Surgery Centre,

16 Ctra. N-521 Km 41.8, 10071, Caceres, Spain.

17 Tel.: +34927181032. Fax: +34927181033

18 rblazquez@ccmijesususon.com

19 **Summary**

20 Endometrial Mesenchymal Stem Cells (endMSCs) reside in the basal and functional layer

21 of human endometrium and participate in tissue remodeling which is required for

22 maintaining the regenerative capacity of the endometrium. The endMSCs are multipotent

23 stem cells and exhibit immunomodulatory effects. This paper aimed to evaluate the

24 regulatory effects of extracellular vesicles derived from endometrial mesenchymal stem

25 cells (EV-endMSCs) in the setting of T cell activation. *In vitro* stimulations of lymphocytes

26 were performed in the presence of EV-endMSCs. These *in vitro* stimulated lymphocytes

27 were functionally and phenotypically characterized to distinguish CD4+ and CD8+ T cell

28 differentiation subsets. Moreover, the inhibition of TGFβ was performed with neutralizing

29 antibodies. The phenotype and nanoparticle tracking analysis of the EV-endMSCs

30 demonstrated that they are similar in terms of size distribution to other MSCs-derived

31 exosomes. The *in vitro* assays showed an immunomodulatory potential of these vesicles to

32 counteract the differentiation of CD4+ T cells. The quantification of active TGFβ in EV-

33 endMSCs was found to be very high when compared to extracellular vesicles-free

34 concentrated supernatants. Finally, the neutralization of TGFβ significantly attenuated the

35 immunomodulatory activity of EV-endMSCs. In summary, this is the first report

36 demonstrating that EV-endMSCs exhibit a potent inhibitory effect against CD4+ T cell

37 activation which is partially mediated by TGFβ signaling.

38 **Keywords:** Extracellular vesicles, Endometrial Mesenchymal Stem Cells,

39 Immunomodulation, TGFβ, Lymphocyte activation, Lymphocyte differentiation.

1. Introduction

The mesenchymal stem/stromal cells (MSCs) have been widely described in bibliography. These cells can be derived from different sources and according to the minimal criteria from the International Society of Cellular Therapy, they are characterized by their plastic adherence, CD73, CD90 and CD105 expression, as well as their differentiation towards osteoblasts, chondroblasts and adipocytes (Dominici *et al.,* 2006).

Multipotent stem cells in endometrial tissue can be obtained by different procedures such as hysterectomy (Wang *et al.,* 2012), endometrial biopsy (Schüring *et al.,* 2011) or by the collection of menstrual blood (Rossignoli *et al.,* 2013) and different names have been given to these multipotent stem cells such as endometrial regenerative cells, endometrial mesenchymal stem-like cells or endometrial decidual tissue multipotent mesenchymal stem cells (Kyurkchiev *et al.,* 2010). According to the hypothesis from E. Lucas *et al.,* endometrial stromal cells, rather than being a homogeneous population, comprise distinct cellular subsets ranging from quiescent and active MSCs (Lucas *et al.,* 2016). Moreover, it is assumed that endometrial MSCs predominantly reside in the perivascular niche of the basal and functional layer maintaining the regenerative capacity of the endometrium (Schwab and Gargett 2007; Masuda *et al.,* 2012).

The isolation of MSCs from the endometrial decidual tissue in menstrual blood is a non-invasive and reproducible method. In contrast to other invasive methods which limit their clinical use, the isolation of endometrial MSCs from menstrual blood (hereinafter referred to as endMSCs) does not require any painful procedure. In terms of laboratory processing,

61   these cells can be selected by plastic adherence and *in vitro* expanded under standard

62   culture conditions. The menstrual blood-derived stromal stem cells display multipotent

63   capabilities and immunomodulatory effects (Nikoo *et al.,* 2012). Moreover, their

64   immunomodulatory capacity have been found to be different when compared women with

65   and without endometriosis (Nikoo *et al.,* 2014).

66   The immunosuppressive mechanisms of endMSCs, as well as the angiogenic and anti-

67   apoptotic, are mainly mediated through paracrine factors. In terms of angiogenic and anti-

68   apopototic factors, VEGF, HGF and IGF-1 have been detected in endMSCs supernatants

69   (Du *et al.,* 2016). With respect to immunosuppressive factors produced by menstrual blood-

70   derived stromal stem cells, indoleamine 2,3-dioxygenase-1 (IDO-1) and cyclooxygenase-2

71   (COX-2) have been described as immunoregulatory molecules (Nikoo *et al.,* 2014).

72   Moreover, Peron et al. demonstrated that endMSCs secrete IL-10 and IL-27 cytokines

73   which are involved in their immunomodulatory effect against Th17 and Th1 T CD4 cells

74   (Peron *et al.,* 2012).

75   Taking into account that the therapeutic effect of MSCs is thought to be mediated by a

76   paracrine effect, the released exosomes and other extracellular vesicles from MSCs have

77   become a promising therapeutic tool for the treatment of inflammatory-related diseases (De

78   Jong *et al.,* 2014; Merino *et al.,* 2014; Zhang *et al.,* 2014). *In vitro* and *in vivo* studies from

79   our laboratory have demonstrated that exosomes derived from mesenchymal stem cells

80   have an immunomodulatory potential against *in vitro* activated T cells (Blazquez *et al.,*

81   2014) as well as an anti-inflammatory effect in an antigen-induced synovitis animal model

82   (G Casado *et al.,* 2017). In two recent papers from Wang K et al. and Chen L et al., it was

83 found that the potent paracrine effect of endMSCs was mediated by secreted exosomes

84 (Chen *et al.,* 2017; Wang *et al.,* 2017). In the first report, a cardioprotective effect (anti-

85 apoptotic and pro-angiogenic) was demonstrated through the release of miR-21 (Wang *et*

86 *al.,* 2017). In the second report, the exosomes from endMSCs showed an anti-apoptotic

87 capacity in the setting of fulminant hepatic failure.

88 In summary, taking into account that the immunomodulatory effect of endMSCs is widely

89 accepted and considering that extracellular vesicles have a key role in the paracrine effect

90 of MSCs, this paper aimed to evaluate the regulatory effect of extracellular vesicles derived

91 from endMSCs (EV-endMSCs) against *in vitro* stimulated T cells. The phenotypic and

92 functional analysis of lymphocyte subsets demonstrated that EV-endMSCs exerted an

93 inhibitory effect counteracting CD4+ T cell activation. More importantly, here we show

94 that these extracellular vesicles are a rich source of active TGFβ and the blockade of TGFβ

95 signaling with neutralizing antibodies showed that the immunomodulatory effect of EV-

96 endMSCs is partially mediated by TGFβ.

97

98 **2. Materials and Methods**

99 **2.1. Isolation and *in vitro* expansion of endometrial MSCs from menstrual blood**

100 Menstrual blood was obtained from four healthy women on day 2 to 3 of the menstrual

101 cycle. Samples were collected using a menstrual cup for several hours. The study was

102 approved by Minimally Invasive Surgery Centre Research Ethics Committee (approval

103   number: SITC215). All participants provided written informed consent. Menstrual blood

104   was diluted 1:2 in PBS and centrifuged at 450 x g for 10 minutes. Supernatant was

105   discarded and the pellet was re-suspended in DMEM (containing 10% FBS, 1%

106   penicillin/streptomycin and 1% glutamine). Subsequently, cells were cultured in a tissue

107   culture flask and expanded at 37 ºC and 5% CO_2. Non-adherent cells were removed after 24

108   h. Adherent cells were cultured to 80% confluency and detached using PBS containing

109   0.25% trypsin. Cells were seeded again into a new culture flask at a density of 5,000

110   cells/cm^2. Culture medium was changed every 4 days.

2.2.   Phenotypic analysis by flow cytometry

112   For phenotypic analysis 2×10^5 cells were stained with human monoclonal antibodies

113   against CD14, CD20, CD34, CD44, CD45, CD73, CD80, CD90, CD117 and HLA-DR and

114   incubated for 30 min at 4 ºC in the presence of PBS containing 2% FBS. The cells were

115   washed and re-suspended in PBS. The corresponding isotype-matched antibodies were used

116   as the negative control. The flow cytometric analysis was performed on a FACScalibur

117   cytometer (BD Biosciences, CA, USA) after acquisition of 10^5 events. Viable cells were

118   selected using forward and side scatter characteristics and analyzed using CellQuest

119   software (BD Biosciences, CA, USA). Isotype-matched negative control antibodies were

120   used in the experiments. The mean relative fluorescence intensity (MRFI) was calculated

121   by dividing the mean fluorescent intensity (MFI) by the MFI of its negative control. Cells

122   were analyzed at passages 3-4.

2.3. Adipogenic, chondrogenic and osteogenic differentiation of endometrial MSCs

from menstrual blood

125   The differentiation assay of endMSCs was performed when the cells reached 80% of

126   confluence. Standard protocols were used to promote osteogenic, adipogenic and

127   chondrogenic differentiation. Cells were cultured for 21 days with differentiation specific

128   media (Gibco Life Sciences, Rockville, MD, USA), which was replaced every three days.

129   Oil Red O, Alcian Blue and Alizarin Red S stainings were performed to evidence

130   adipogenic, chondrogenic and osteogenic differentiation, respectively. The degree of

131   adipogenic, chondrogenic and osteogenic differentiations was quantified by determining the

132   absorbance of the extracts at 490 nm (Oil Red O and Alizarin Red S staining) and at 600

133   nm (Alcian Blue 8GX). Alcian blue and Alizarin Red staining were extracted with 6 M

134   guanidine-HCl. Oil Red O staining was extracted with pure isopropanol.

135   **2.4. Isolation, purification and characterization of EV-endMSCs**

136   The mesenchymal stem cells-derived extracellular vesicles were obtained from endMSCs

137   cultured in 175 cm^2 flasks. When cells reached a confluence of 80%, culture medium

138   (DMEM containing 10% FBS) was replaced by exosome isolation medium (DMEM

139   containing 1% insulin-transferrin-selenium). The supernatants were collected every 3-4

140   days. To eliminate dead cells and debris, the supernatants were centrifuged at 1,000 x g for

141   10 min and 5,000 x g for 20 min at 4 °C. Every 15 ml of these supernatants were ultra-

142   filtered through a 3 kDa MWCO Amicon® Ultra device (Merck-Millipore, MA, USA).

143   Samples were spun at 4,000 x g for 60 min and 200-300 µl of concentrated supernatant

144　were collected and stored at -20 °C. To obtain the EV-Free concentrated supernatants, the

145　concentrated supernatants were ultracentrifuged for 2 hours at 100,000 x g and stored at -20

146　°C.

147　Prior to *in vitro* experiments, extracellular vesicle concentration was indirectly quantified

148　by protein measurements in a Bradford assay. Moreover, a nanoparticle tracking analysis

149　(NanoSight Ltd, Amesbury, UK) was also performed to characterize the size and to

150　quantify the number of particles per milliliter. Results were analyzed using the nanoparticle

151　tracking analysis software package version 2.2. Triplicate samples were diluted 1:100,

152　1:500 and 1:1000 in sterile-filtered PBS and analyzed.

153　For flow cytometric analysis, extracellular vesicles were conjugated with latex beads.

154　Briefly, 5 µg of extracellular vesicles were incubated 15 min at room temperature with 10

155　µl of aldehyde/Sulfate latex beads (4 µm) (Molecular probes, Life Technologies, Carlsbad,

156　CA, USA). PBS was then added to a final volume of 1 ml and samples were incubated

157　overnight at 4 ºC. Finally, 110 µl of 1 M glycine were added to each tube. After 30 min of

158　incubation, samples were centrifuged, washed and re-suspended in a final volume of 0.5 ml

159　PBS/0.5% BSA. These extracellular vesicles-coated beads were incubated for 1 h at room

160　temperature with human monoclonal antibodies against CD9 and CD63 (BD Biosciences,

161　San Jose, CA, USA). After incubation, the extracellular vesicles-coated beads were washed

162　and re-suspended in PBS/0.5% BSA. The flow cytometric analysis was performed on a

163　FACScalibur cytometer (BD Biosciences, San Jose, CA, USA) after acquisition of 10^5

164　events. The extracellular vesicles-bead complexes were primarily selected using forward

165　and side scatter characteristics and fluorescence was analyzed using CellQuest software

166 (BD Biosciences). Isotype-matched negative control antibodies were used in all the
167 experiments.

168 For proteomics analysis, protein extracts were incubated with trypsin using the Filter Aides
169 Sample Preparation (FASP) digestion kit (Expedeon), as previously described (Wiśniewski
170 *et al.*, 2011). The resulting peptides were labelled using 8plex-iTRAQ reagents (Sciex)
171 according to manufacturer´s instructions and desalted on OASIS HLB extraction cartridges
172 (Waters Corp.). Half of the tagged peptides were directly analyzed by LC-MS in different
173 acquisition runs, and the remaining peptides were separated into 3 fractions using the high
174 pH reversed-phase peptide fractionation kit (Thermo Fisher Scientific). High-resolution
175 LC-MS analysis of iTRAQ-labelled peptides was carried out on an Easy nLC 1000 nano-
176 HPLC apparatus (Thermo Scientific) coupled to QExactive mass spectrometer (Thermo
177 Fisher Scientific). Peptides were injected onto a C18 reversed phase (RP) nano-column (75
178 µm I.D. and 50 cm, Acclaim PepMap100, Thermo Scientific) in buffer A (0.1% formic acid
179 (v/v)) and eluted with a 180 min lineal gradient of buffer B (90% acetonitrile, 0.1% formic
180 acid (v/v)). MS runs consisted of enhanced FT-resolution spectra (140,000 resolution) in
181 the 390-1,500 m/z range and separated 390-700, 650-900, and 850-1500 m/z ranges
182 followed by data-dependent MS/MS spectra of the 15 most intense parent ions acquired
183 along the chromatographic run. HCD fragmentation was performed at 30% of normalized
184 collision energy. A total of 14 MS data sets, eight from unfractionated material and six
185 from the corresponding fractions, were registered with 42 h total acquisition time. For
186 peptide identification the MS/MS spectra were searched with the SEQUEST HT algorithm
187 implemented in Proteome Discoverer 2.1 (Thermo Scientific). The results were analyzed

9

188 using the probability ratio method (Martinez-Bartolome *et al*., 2008) and the false

189 discovery rate (FDR) of peptide identification was calculated based on the search results

190 against a decoy database using the refined method (Navarro *et al*., 2009). Enrichment

191 analysis was performed by using the DAVID functional annotation database

192 (https://david.ncifcrf.gov/).

193 **2.5. Measurements of active TGFβ by ELISA**

194 The quantification of TGFβ1 was performed by ELISA test using the LEGEND MAX^{TM}

195 Free active TGFβ1 (Biolegend, San Diego, CA) and according to the manufacturer's

196 instructions. The active form of TGFβ was quantified in the extracellular vesicles-free

197 fractions from extracellular vesicle-enriched supernatants. Additionally, the active TGFβ

198 was quantified in the extracellular vesicle-containing fraction of ultracentrifuged

199 supernatants. Both lysed and intact extracellular vesicles were quantified and TGFβ was

200 normalized on the basis of total protein content. The vesicles were lysed with 0.05%

201 Tween-20 and 2.5% Triton at pH 7.4.

202 **2.6. Lymphocytes isolation**

203 Peripheral blood lymphocytes (PBLs) were obtained from healthy adult donors by

204 centrifugation of peripheral blood collected in EDTA over Histopaque-1077 (Sigma, St.

205 Louis, MO, USA) and washed twice with PBS. The PBLs was re-suspended in RPMI 1640

206 supplemented with 10% FBS.

207

208 **2.7. *In vitro* stimulation of PBLs and co-culture with EV-endMSCs**

209 To determine the immunomodulatory effect of EV-endMSCs on *in vitro* stimulated PBLs, a

210 total of $2x10^5$ PBLs/well were seeded in a 96 wells plate. In order to stimulate PBLs, a T

211 cell activation/expansion kit was used (Miltenyi Biotec Inc, San Diego, CA, USA).

212 Extracellular vesicles at different concentrations (8, 16, and 32 $\times10^{10}$ particles/ml) were

213 added to different wells. The PBLs and extracellular vesicles were co-cultured for 3 and 6

214 days. Negative controls (non-stimulated PBLs) and positive controls (stimulated PBLs

215 without extracellular vesicles) were used in all the experiments. In a second set of

216 experiments, the TGFβ blockade was performed using a TGFβ-neutralizing antibody (clone

217 1D11) at 1 μg/ml (Thermo Fisher Scientific, Waltham, MA, USA).

218 **2.8. Differentiation/activation markers expression on *in vitro* stimulated PBLs**

219 For flow cytometry, *in vitro* stimulated PBLs co-cultured with extracellular vesicles at

220 different concentrations (8, 16, and 32 $\times10^{10}$ particles/ml) with or without TGFβ-

221 neutralizing antibodies were collected at day 6. The cells were stained with fluorescence-

222 labeled human monoclonal antibodies against CD4 (SK3), CD8 (SK1), CD62L (DREG-56)

223 and CD45RA (L48) (BD Biosciences, San Jose, CA, USA). The cytometric analysis was

224 performed as follows: $2x10^5$ cells were incubated for 30 min at 4 °C with appropriate

225 concentrations of monoclonal antibodies in the presence of PBS containing 2% FBS. The

226 cells were washed and re-suspended in PBS. The flow cytometric analysis was performed

227 on a FACScalibur cytometer and analyzed using Cell Quest software (BD Biosciences, San

228 Jose, CA, USA) after acquisition of 10^4 events. Viable cells were selected using forward

229   and side scatter characteristics and fluorescence was analyzed using CellQuest software

230   (BD Biosciences, CA, USA). Isotype-matched negative control antibodies and/or

231   Fluorescence Minus One (FMO) controls were used in the experiments.

232   **2.9. Statistical analysis**

233   Data were statistically analyzed with SPSS-21 software (SPSS, Chicago, IL, USA). Normal

234   distribution of variables, as well as homoscedasticity, was firstly assessed using Shapiro-

235   Wilk and Levene tests, respectively. For variables with normal distribution and

236   homogeneity of variances, one-way ANOVA test was performed. When a statistically

237   significant difference was found, a Tukey test was performed to evidence differences

238   between groups. For non-parametric and heteroscedastic variables, a Kruskal-Wallis test

239   was performed, followed by a Dunn's test to evidence differences between groups. The p-

240   values ≤0.05 were considered statistically significant.

241

242   **3. Results**

243   **3.1. Phenotypic analysis of endMSCs**

244   Menstrual blood was collected from four healthy donors. Plastic adherent cells were *in vitro*

245   expanded at 5,000 cell/cm^2 and the population doubling time of these cells was between 48

246   and 72 hours. The endMSCs cultured under standard conditions were characterized by flow

247   cytometry. The phenotypic analysis, demonstrated that endMSCs were negative for CD14,

248   CD20, CD34, CD45, CD80, HLA-DR and positive for the stemness markers CD44, CD73,

249 CD90 and CD117. Figure 1A shows the representative histograms for these markers and

250 the numbers within the histograms represent the mean and standard deviation of MRFI

251 from different donors (n=4). It is interesting to note that we did not observe significant

252 changes in the phenotype of endMSCs after different passages and their phenotypes were

253 very similar when different donors were compared (data not shown).

254 In order to demonstrate the multipotency of isolated and *in vitro* expanded endMSCs, the

255 adipogenic, chondrogenic and osteogenic differentiation potential was evaluated according

256 to standard differentiation protocols. The endMSCs were cultured for 21 days and

257 differentiation was evaluated with Alizarin Red, Alcian Blue and Oil Red O stainings. The

258 stains were solubilized and the resulting absorbances were quantified by spectrophotometry

259 (Figure 1B). As shown in the representative images, the differentiation towards adipogenic,

260 chondrogenic and osteogenic lineages was confirmed by microscopy (Figure 1C).

261 **3.2. Size distribution, concentration and characterization of EV-endMSCs**

262 The cell culture supernatants from endMSCs (n=4) were enriched up to 50 times with

263 centrifugal filter concentration devices. The quantification of proteins in extracellular

264 vesicle-enriched supernatants was performed by Bradford assay. The resulting protein

265 concentrations ranged between 350 and 750 μg/ml.

266 Additionally, in order to fully characterize these extracellular vesicles, a nanoparticle

267 tracking analysis was performed for each cell line (n=4). This analysis allowed us to

268 quantify size distribution and particle concentration. The mean size and standard deviation

269 of isolated vesicles was 153.5±63.05 nm. The concentration was $3.31\times10^{11}\pm3.8\times10^{9}$

270   particles/ml. Figure 2A shows a representative analysis of nanoparticle tracking. Finally,

271   exosomal markers were identified by flow cytometry. Our results demonstrated that

272   different extracellular vesicles isolated from four different endMSCs were positive for CD9

273   and CD63. Figure 2B shows representative histograms for these markers.

274   Regarding the high-throughput proteomic analysis, a total of 657 proteins (with more than

275   two peptides per protein at 1% FDR) were identified in the EV-endMSCs. Among these

276   657 selected proteins, 480 (75%) were associated to the Gene Ontology term *extracellular*

277   *exosome* (GO:0070062, p<<<0.001, 1% FDR) and 62 of them were present in the 100 top

278   identified proteins in Exo Carta database (Keerthikumar *et al.*, 2015) (Figure 2C).

279   **3.3. Distribution of *in vitro* stimulated T cells co-cultured in the presence of EV-**
280   **endMSCs**

281   In order to study the effect of EV-endMSCs over lymphocyte subsets, a total of $2x10^5$ *in*

282   *vitro* stimulated PBLs (isolated from four healthy donors) were co-cultured in the presence

283   of four different EV-endMSCs. These extracellular vesicles were co-cultured *in vitro* with

284   PBLs at 8, 16 and 32 $\times10^{10}$ particles/ml. At day 6, multiparametric flow cytometry was

285   performed on gated CD4+ and CD8+ T cells and the co-expression of CD45RA and

286   CD62L was analyzed to distinguish T cell differentiation subsets.

287   As expected, our results firstly showed a significant decrease of CD4+ naïve T cells

288   (CD45RA+ and CD62L+) in the positive control (CON) when compared to non-stimulated

289   PBLs (Figure 3A). This decrease of naïve cells on *in vitro* stimulated PBLs was

290   significantly compensated by the presence of EV-endMSCs at 16 and 32 $\times10^{10}$ particles /ml

14

291   (Figure 3A). Simultaneously, the increase in *in vitro* stimulated effector memory CD4+ T

292   cells was also compensated by the presence of EV-endMSCs and despite extracellular

293   vesicle concentration (Figure 3B).

294   Regarding *in vitro* stimulated CD8+ T cells, no significant changes were observed in naïve

295   (Figure 3C) or effector memory (Figure 3D) T cells subsets.

296   Additionally, in order to exclude the possibility that the immunomodulatory effect observed

297   on CD4+ T cells with the extracellular vesicle-enriched supernatants was not attributed to

298   soluble factors (not contained in EV-endMSCs), *in vitro* stimulated PBLs were co-cultured

299   with ultracentrifuged enriched supernatants, also called extracellular vesicle-free fractions,

300   from different donors. As shown in Supplementary Figure 1, any statistical difference was

301   observed between the positive control and those PBLs co-cultured with the extracellular

302   vesicle-free fractions. It is important to note that, in this analysis, equivalent concentrations

303   of soluble protein to extracellular vesicle proteins were used.

304   **3.4. Active TGFβ in EV-endMSCs: analysis on EV-free fractions and**

305   **ultracentrifuged fractions**

306   In order to determine the levels of active TGFβ in EV-endMSCs, samples from four

307   different donors were ultracentrifuged. This procedure allowed us to quantify the TGFβ in

308   the EV-free fraction. The quantification of active TGFβ in EV-free fraction demonstrated

309   that soluble TGFβ (normalized on the basis of total protein content) is very low (Figure 4,

310   left column). In contrast, ultracentrifugation allowed us to obtain a purified fraction of

311   extracellular vesicles which showed high levels of active TGFβ. Moreover, it is important

312   to note that TGFβ was also quantified in intact and lysed extracellular vesicles. This

313   analysis demonstrated the presence of surface-bound TGFβ in extracellular vesicles as well

314   as its encapsulation in the vesicles (Figure 4).

315   **3.5. TGFβ blockade on EV-endMSCs and co-culture with *in vitro* stimulated T cells**

316   The impact of TGFβ blockade in the immunomodulatory activity of extracellular vesicles

317   was evaluated using TGFβ neutralizing antibodies. These neutralizing antibodies were pre-

318   incubated with EV-endMSCs and co-cultured with PBLs during *in vitro* stimulation. At day

319   6, the co-expression of CD45RA and CD62L was analyzed in CD4+ T cells and CD8+ T

320   cells. The percentage of naïve T cells (CD45RA+ CD62L+) and effector memory T cells

321   (CD45RA–CD62L–) were compared to the positive control (CON) both in control samples

322   and in TGFβ blockade samples. It is important to note that, in order to analyze whether the

323   difference between the positive controls (with and without TGFβ blockade) could interfere

324   in the analysis, additional statistical analyses were carried out to evidence potential

325   differences between them.

326   Our results showed that TGFβ blockade partially counteracted the immunomodulatory

327   effect of extracellular vesicles against *in vitro* activated CD4+ T cells (Figure 5A and 5B).

328   As expected, no significant differences were found in CD8+ T cells, where no

329   immunomodulatory effect was initially observed (Figure 5C and 5D).

330

331   **4. Discussion**

332   Endometrial stem cells reside in the perivascular niche of the basal and functional layer of

333   human endometrium maintaining the regenerative capacity of the tissue (Gargett *et al.,*

334   2016). These cells migrate towards the functional layer during the menstrual cycle and

335   participate in tissue remodeling which is required for the reconstruction of the endometrium

336   (Elsheikh *et al.,* 2011). Although the bibliography shows different classifications,

337   according to the review by Gargett et al., resident stem cells in the human endometrium

338   could be classified as three different subsets: epithelial stem cells, endothelial stem cells

339   and mesenchymal stem cells (Gargett *et al.,* 2012). In comparison to other stem cells such

340   as adipose-derived stem cells or bone marrow-derived stem cells, the isolation method of

341   endometrial stem cells from shed blood is a non-invasive practice and does not require any

342   painful procedure. These cells can be selected by adherence and have been found to be very

343   similar, at least in terms of phenotype, to other MSCs from different sources (Patel *et al.,*

344   2008).

345   Considering that endometrial MSCs have shown immunomodulatory effects (as well as

346   angiogenesis and vascularization during tissue remodeling), this paper aimed to evaluate

347   the immunomodulatory effects of extracellular vesicles from endometrial mesenchymal

348   stem cells (EV-endMSCs) against *in vitro* stimulated T cells. Our first sets of experiments

349   were carried out to isolate, expand and characterize endMSCs from healthy donors. Four

350   out of four cell lines were successfully expanded and similar to previous published studies,

351   these cells showed a highly proliferative rate and a very short population doubling time

352   (Rossignoli *et al.,* 2013). The phenotypic analysis of these cells was also very similar to

353   MSCs from other sources such as adipose-derived MSCs or bone marrow-derived MSCs

354 (Sousa *et al.,* 2014). Moreover, our endMSCs showed phenotypical similarities to

355 previously characterized endometrial stem cells named as endometrial decidual tissue

356 multipotent mesenchymal stem cells (Rossignoli *et al.,* 2013), endometrial mesenchymal

357 stem-like cells (Schüring *et al.,* 2011) or menstrual blood-derived stromal stem cells (Nikoo

358 *et al.,* 2012). Once the phenotype of endMSCs was characterized, the *in vitro*

359 differentiation towards adipogenic, chondrogenic and osteogenic lineages was found to be

360 similar to previously published results using endometrial stem cells (Du *et al.,* 2016).

361 Based on previously described protocols from our group (Álvarez *et al.,* 2015), the EV-

362 endMSCs were successfully isolated and the distribution size was comparable to exosomes

363 isolated from other cell sources (G Casado *et al.,* 2017). The immunomodulatory role of

364 EV-endMSCs was evaluated in *in vitro* stimulated T cell subsets using anti-CD2, anti-CD3

365 and anti-CD28 that partially mimic the stimulation by antigen-presenting cells (Figure 6A)

366 (Trickett and Kwan, 2003). The co-expression analysis of CD45RA and CD62L in *in vitro*

367 stimulated T cells allowed us to identify four major subsets with distinct functional

368 properties: naïve (CD45RA+ CD62L+), central memory (CM) (CD45RA–CD62L+),

369 effector memory (EM) (CD45RA–CD62L–) and effector memory re-expressing CD45RA

370 (TEMRA) (CD45RA+CD62L–) cells (Maldonado *et al.,* 2003; Foster *et al.,* 2004; Turtle *et*

371 *al.,* 2009; Pender *et al.,* 2014; Prabhu *et al.,* 2016; Golubovskaya and Wu 2016). Similar to

372 previous findings using extracellular vesicles from adipose-derived MSCs (Blazquez *et al.,*

373 2014), our results demonstrated that EV-endMSCs significantly inhibited *in vitro*-induced

374 differentiation of CD4+ T cells towards effector memory cells. The Figure 6B represents

375 the co-culture of EV-endMSCs with *in vitro* stimulated PBLs and the inhibitory effect of

376 these vesicles on CD4+ T cell differentiation. Our results are in agreement with a previous

377 study by Wang *et al.* who demonstrated in endometrial regenerative cells (ERCs) an

378 overexpression of released soluble factors with a greater immunomodulatory potential

379 against T cells when compared to bone marrow-derived MSCs (Wang *et al.,* 2012). It is

380 necessary to clarify that, Wang et al. evaluated the gene expression of ERCs and the

381 presence of soluble factors in cell supernatants, but not in extracellular vesicles. In our

382 experimental setting, the soluble factors from extracellular vesicle-free fractions did not

383 show any significant immunomodulatory effect against anti-CD2, anti-CD3 and anti-CD28

384 stimulated T cell subsets. However, we should consider that these soluble factors may exert

385 a regulatory effect under different stimulation conditions.

386 In order to identify the key regulatory molecules involved in the immunomodulatory

387 capacity of these EV-endMSCs, we hypothesized that TGFβ would be directly involved in

388 the immunomodulatory activity of these vesicles. This hypothesis was based on four

389 different types of evidence. Firstly, TGFβ participates in the onset of menstruation and all

390 three TGFβs are increased around menstruation (Omwandho *et al.,* 2010). Secondly, the

391 identification of TGFβ and receptors in endometrial cells appears to be associated with cell

392 proliferation, differentiation, apoptosis and tissue remodeling (Jones *et al.,* 2006). Thirdly,

393 TGFβ has been found to be contained in exosomes from different cells such as epithelial

394 cells (Borges *et al.,* 2013) or cancer cells (Webber *et al.,* 2010). Finally, this cytokine has

395 been found to be released by adult stem cells as adipose-derived MSCs (inducing Treg

396 expansion) (Cho *et al.,* 2015) or autologous MSCs (as a modulator of microglia) (Noh *et*

397 *al.,* 2016).

398   The quantification of active TGFβ1, demonstrated that EV-endMSCs contained high levels

399   of this cytokine which may suggest a hypothetical inhibitory effect of these extracellular

400   vesicles through TGFβ signaling. Moreover, the ELISA test demonstrated the presence of

401   surface-bound TGFβ and encapsulated TGFβ in extracellular vesicles. Based on these

402   results, anti-TGFβ blocking experiments with the neutralizing antibody 1D11 (Dasch *et al.,*

403   1989) were performed to identify any hypothetical evidence for a link between

404   immunosuppresive effects and TGFβ levels. The results from these studies /Figure 5) are

405   summarized in Figure 6C which schematically shows the effect of TGFβ blocking in the

406   immunomodulatory capacity of extracellular vesicles on CD4+ T cells. Our *in vitro*

407   differentiation-activation assays in the presence of extracellular vesicles TGFβ neutralized

408   are in agreement with Murphy *et al.* who demonstrated that Conditioned Media and

409   Endometrial Regenerative Cells co-cultured with peripheral blood leukocytes suppressed

410   their TNFα and IFNγ production (Murphy *et al.,* 2008).

411   TGFβ release from adult stem cells has been found to be related to breast cancer

412   progression where adipose-derived stem cells triggered a potent anti-inflammatory response

413   in the tumor site through TGFβ signaling (Razmkhah *et al.,* 2011). According to our

414   results, we have proved that endMSCs may share similarities in terms of

415   immunomodulatory mechanisms with tumor tissue-resident stem cells. Additionally,

416   although this study has been only limited to the immunomodulatory effect against T cells,

417   we should not discard a hypothetical effect of EV-endMSCs and TGFβ against other

418   immune cells. Moreover, we should also consider that, apart from TGFβ, other potential

419   candidates (i.e. indoleamine 2,3-dioxygenase, miRNAs, proteins, lipids and RNAs) may

420   simultaneously participate in the inhibitory effect of these vesicles. Finally, it is interesting

421   to note that previous reports have also shown that MSC-conditioned media modulate the

422   response of CD68+ immune cells through TGFβ (Yoo *et al.,* 2013) and that TGFβ released

423   by MSCs, acts by autocrine mechanisms which seems to reverse the immunosuppressive

424   effect of these cells (Xu *et al.,* 2014).

425   In conclusion, to our knowledge, this is the first report demonstrating that EV-endMSCs

426   had a potent inhibitory effect against CD4+ T cell activation and differentiation. These

427   extracellular vesicles showed a large quantity of active TGFβ and have been experimentally

428   proved to be associated with their immunomodulatory activity.

429

5. Acknowledgments

448

6. Conflict of interest statement

450 The authors declare that this research was conducted in the absence of any commercial or

451 financial relationships that could be construed as a potential conflict of interest.

452

7. References

454 Álvarez V, Blázquez R, Sánchez-Margallo FM, DelaRosa O, Jorge I, Tapia A, Casado JG

455   2015, Comparative study of isolated human mesenchymal stem cell derived

456   exosomes for clinical use, *Acta bioquim clin latinoam,* **49**: 311–320

457 Blazquez R, Sanchez-Margallo FM, de la Rosa O, Dalemans W, Alvarez V, Tarazona R,

458   Casado JG. 2014, Immunomodulatory Potential of Human Adipose Mesenchymal

459   Stem Cells Derived Exosomes on in vitro Stimulated T Cells, *Front Immunol,* **5**:

460   556. doi:10.3389/fimmu.2014.00556.

461 Borges FT, Melo SA, Özdemir BC, Kato N, Revuelta I, Miller CA, Gattone VH, LeBleu

462   VS, Kalluri R. 2013, TGF-β1-containing exosomes from injured epithelial cells

463   activate fibroblasts to initiate tissue regenerative responses and fibrosis, *J Am Soc*

464   *Nephrol,* **24**: 385–392. doi:10.1681/ASN.2012101031.

465 Chen L, Xiang B, Wang X, Xiang C. 2017, Exosomes derived from human menstrual

466   blood-derived stem cells alleviate fulminant hepatic failure, *Stem Cell Res Ther,* **8**:

467   9. doi:10.1186/s13287-016-0453-6.

468 Cho K-S, Lee J-H, Park M-K, Park H-K, Yu H-S, Roh H-J. 2015, Prostaglandin E2 and

469   Transforming Growth Factor-β Play a Critical Role in Suppression of Allergic

470   Airway Inflammation by Adipose-Derived Stem Cells, *PLoS One,* **10**: e0131813.

471   doi:10.1371/journal.pone.0131813.

472 Dasch JR, Pace DR, Waegell W, Inenaga D, Ellingsworth L. 1989, Monoclonal antibodies

473   recognizing transforming growth factor-beta. Bioactivity neutralization and

474   transforming growth factor beta 2 affinity purification, *J Immunol,* **142**: 1536–1541.

475 De Jong OG, Van Balkom BWM, Schiffelers RM, Bouten CVC, Verhaar MC. 2014,

476   Extracellular vesicles: potential roles in regenerative medicine, *Front Immunol,* **5**:

477   608. doi:10.3389/fimmu.2014.00608.

478   Dominici M, Blanc KL, Mueller I, Slaper-Cortenbach I, Marini FC, Krause DS, Deans RJ,

479   Keating A, Prockop DJ, Horwitz EM. 2006, Minimal criteria for defining

480   multipotent mesenchymal stromal cells. The International Society for Cellular

481   Therapy position statement, *Cytotherapy,* **8**: 315–317.

482   doi:10.1080/14653240600855905.

483   Du X, Yuan Q, Qu Y, Zhou Y, Bei J. 2016, Endometrial Mesenchymal Stem Cells Isolated

484   from Menstrual Blood by Adherence, *Stem Cells Int,* **2016**: 3573846.

485   doi:10.1155/2016/3573846.

486   Elsheikh E, Sylvén C, Ericzon B-G, Palmblad J, Mints M. 2011, Cyclic variability of

487   stromal cell-derived factor-1 and endothelial progenitor cells during the menstrual

488   cycle, *Int J MolMed,* **27**: 221–226. doi:10.3892/ijmm.2010.570.

489   Foster AE, Marangolo M, Sartor MM, Alexander SI, Hu M, Bradstock KF, Gottlieb DJ.

490   2004, Human CD62L- memory T cells are less responsive to alloantigen stimulation

491   than CD62L+ naive T cells: potential for adoptive immunotherapy and

492   allodepletion, *Blood,* **104**: 2403–2409. doi:10.1182/blood-2003-12-4431.

493   G Casado J, Blázquez Durán R, Vela FJ, Álvarez Pérez V, Tarazona R, Margallo S, M F.

494   2017, Mesenchymal stem cells derived exosomes: immunomodulatory evaluation in

495   an antigen-induced synovitis porcine model, *Front Vet Sci,* **4**.

496   doi:10.3389/fvets.2017.00039.

497   Gargett CE, Nguyen HPT, Ye L. 2012, Endometrial regeneration and endometrial
498   stem/progenitor cells, *Rev Endocr Metab Disord,* **13**: 235–251. doi:10.1007/s11154-
499   012-9221-9.

500   Gargett CE, Schwab KE, Deane JA. 2016, Endometrial stem/progenitor cells: the first 10
501   years. *Hum Reprod Update,* **22**: 137–163. doi:10.1093/humupd/dmv051.

502   Golubovskaya V, Wu L. 2016, Different Subsets of T Cells, Memory, Effector Functions,
503   and CAR-T Immunotherapy, *Cancers (Basel),* **8**: 36. doi:10.3390/cancers8030036.

504   Jones RL, Stoikos C, Findlay JK, Salamonsen LA. 2006, TGF-beta superfamily expression
505   and actions in the endometrium and placenta, *Reproduction,* **132**: 217–232.
506   doi:10.1530/rep.1.01076.

507   Keerthikumar S, Chisanga D, Ariyaratne D, Al Saffar H, Anand S, Zhao K, Samuel M,
508   Pathan M, Jois M, Chilamkurti N, Gangoda L, Mathivanan S. 2015, ExoCarta: A
509   web-based compendium of exosomal cargo. *J Mol Biol*, **428**: 688–692. doi:
510   10.1016/j.jmb.2015.09.019.

511   Kyurkchiev S, Shterev A, Dimitrov R. 2010, Assessment of presence and characteristics of
512   multipotent stromal cells in human endometrium and decidua, *Reprod Biomed*
513   *Online,* **20**: 305–313. doi:10.1016/j.rbmo.2009.12.011.

514   Lucas ES, Dyer NP, Fishwick K, Ott S, Brosens JJ. 2016, Success after failure: the role of
515   endometrial stem cells in recurrent miscarriage, *Reproduction,* **152**: R159-166.
516   doi:10.1530/REP-16-0306.

517   Maldonado A, Mueller YM, Thomas P, Bojczuk P, O'Connors C, Katsikis PD. 2003,

518   Decreased effector memory CD45RA+ CD62L- CD8+ T cells and increased central

519   memory CD45RA- CD62L+ CD8+ T cells in peripheral blood of rheumatoid

520   arthritis patients, *Arthritis Res Ther,* **5**: R91–R96.

521   Martinez-Bartolome S, Navarro P, Martin-Maroto F, Lopez-Ferrer D, Ramos-Fernandez A,

522   Villar M, Garcia-Ruiz JP, Vazquez J. 2008, Properties of average score distributions

523   of SEQUEST: The probability ratio method. *Mol Cell Proteomics*, **7**: 1135−1145.

524   doi: 10.1074/mcp.M700239-MCP200.

525   Masuda H, Anwar SS, Bühring H-J, Rao JR, Gargett CE. 2012, A novel marker of human

526   endometrial mesenchymal stem-like cells, *Cell Transplant,* **21**: 2201–2214.

527   doi:10.3727/096368911X637362.

528   Merino AM, Hoogduijn MJ, Borras FE, Franquesa M. 2014, Therapeutic Potential of

529   Extracellular Vesicles. *Front Immunol,* **5**: 658. doi:10.3389/fimmu.2014.00658.

530   Murphy MP, Wang H, Patel AN, Kambhampati S, Angle N, Chan K, Marleau AM,

531   Pyszniak A, Carrier E, Ichim TE, Riordan NH. 2008, Allogeneic endometrial

532   regenerative cells: an 'Off the shelf solution' for critical limb ischemia?, *J Transl*

533   *Med,***6**: 45. doi:10.1186/1479-5876-6-45.

534   Navarro P, Vázquez J. 2009, A refined method to calculate false discovery rates for peptide

535   identification using decoy databases. *J Proteome Res*, **8**: 1792-1796.

536   Nikoo S, Ebtekar M, Jeddi-Tehrani M, Shervin A, Bozorgmehr M, Kazemnejad S, Zarnani

537   AH. 2012, Effect of menstrual blood-derived stromal stem cells on proliferative

538   capacity of peripheral blood mononuclear cells in allogeneic mixed lymphocyte

539   reaction, *J Obstet Gynaecol Res,* **38**: 804–809. doi:10.1111/j.1447-

540   0756.2011.01800.x.

541   Nikoo S, Ebtekar M, Jeddi-Tehrani M, Shervin A, Bozorgmehr M, Vafaei S, Kazemnejad

542   S, Zarnani A-H. 2014, Menstrual blood-derived stromal stem cells from women

543   with and without endometriosis reveal different phenotypic and functional

544   characteristics, *Mol Hum Reprod,* **20**: 905–918. doi:10.1093/molehr/gau044.

545   Noh MY, Lim SM, Oh K-W, Cho K-A, Park J, Kim K-S, Lee S-J, Kwon M-S, Kim SH.

546   2016, Mesenchymal Stem Cells Modulate the Functional Properties of Microglia

547   via TGF-β Secretion, *Stem Cells Transl Med,* **5**: 1538–1549.

548   doi:10.5966/sctm.2015-0217.

549   Omwandho COA, Konrad L, Halis G, Oehmke F, Tinneberg H-R. 2010, Role of TGF-betas

550   in normal human endometrium and endometriosis, *Hum Reprod,* **25**: 101–109.

551   doi:10.1093/humrep/dep382.

552   Patel AN, Park E, Kuzman M, Benetti F, Silva FJ, Allickson JG. 2008, Multipotent

553   menstrual blood stromal stem cells: isolation, characterization, and differentiation,

554   *Cell Transplant,* **17**: 303–311.

555 Pender MP, Csurhes PA, Pfluger CM, Burrows SR. 2014, Deficiency of CD8+ effector
556   memory T cells is an early and persistent feature of multiple sclerosis, J *Mult Scler,*
557   **20**: 1825–1832. doi:10.1177/1352458514536252.

558 Peron JPS, Jazedje T, Brandão WN, Perin PM, Maluf M, Evangelista LP, Halpern S,
559   Nisenbaum MG, Czeresnia CE, Zatz M, Câmara NOS, Rizzo LV. 2012, Human
560   endometrial-derived mesenchymal stem cells suppress inflammation in the central
561   nervous system of EAE mice, *Stem Cell Rev,* **8**: 940–952. doi:10.1007/s12015-011-
562   9338-3.

563 Prabhu SB, Rathore DK, Nair D, Chaudhary A, Raza S, Kanodia P, Sopory S, George A,
564   Rath S, Bal V, Tripathi R, Ramji S, Batra A, Aggarwal KC, Chellani HK, Arya S,
565   Agarwal N, Mehta U, Natchu UCM, Wadhwa N, Bhatnagar S. 2016, Comparison of
566   Human Neonatal and Adult Blood Leukocyte Subset Composition Phenotypes,
567   *PLoS One,* **11**: e0162242. doi:10.1371/journal.pone.0162242.

568 Razmkhah M, Jaberipour M, Erfani N, Habibagahi M, Talei A, Ghaderi A. 2011, Adipose
569   derived stem cells (ASCs) isolated from breast cancer tissue express IL-4, IL-10 and
570   TGF-β1 and upregulate expression of regulatory molecules on T cells: do they
571   protect breast cancer cells from the immune response?, *Cell Immunol,* **266**: 116–
572   122. doi:10.1016/j.cellimm.2010.09.005.

573 Rossignoli F, Caselli A, Grisendi G, Piccinno S, Burns JS, Murgia A, Veronesi E, Loschi P,
574   Masini C, Conte P, Paolucci P, Horwiz EM, Dominici M. 2013, Isolation,
575   Characterization, and Transduction of Endometrial Decidual Tissue Multipotent

576   Mesenchymal Stromal/Stem Cells from Menstrual Blood, *BioMed Res Int,* **2013**.

577   doi:10.1155/2013/901821.

578   Schüring AN, Schulte N, Kelsch R, Röpke A, Kiesel L, Götte M. 2011, Characterization of

579   endometrial mesenchymal stem-like cells obtained by endometrial biopsy during

580   routine diagnostics, *Fertil Steril,* **95**: 423–426. doi:10.1016/j.fertnstert.2010.08.035.

581   Schwab KE, Gargett CE. 2007, Co-expression of two perivascular cell markers isolates

582   mesenchymal stem-like cells from human endometrium, *Hum Reprod,* **22**: 2903–

583   2911. doi:10.1093/humrep/dem265.

584   Sousa BR, Parreira RC, Fonseca EA, Amaya MJ, Tonelli FMP, Lacerda SMSN, Lalwani P,

585   Santos AK, Gomes KN, Ulrich H, Kihara AH, Resende RR. 2014, Human adult

586   stem cells from diverse origins: An overview from multiparametric

587   immunophenotyping to clinical applications, *Cytometry A,* **85**: 43–77.

588   doi:10.1002/cyto.a.22402.

589   Trickett A, Kwan YL. 2003, T cell stimulation and expansion using anti-CD3/CD28 beads,

590   *J immunol methods,* **275**: 251–255. doi:10.1016/S0022-1759(03)00010-3.

591   Turtle CJ, Swanson HM, Fujii N, Estey EH, Riddell SR. 2009, A distinct subset of self-

592   renewing human memory CD8+ T cells survives cytotoxic chemotherapy,

593   *Immunity,* **31**: 834–844. doi:10.1016/j.immuni.2009.09.015.

594   Wang K, Jiang Z, Webster KA, Chen J, Hu H, Zhou Y, Zhao J, Wang L, Wang Y, Zhong

595   Z, Ni C, Li Q, Xiang C, Zhang L, Wu R, Zhu W, Yu H, Hu X, Wang J 'an. 2017,

Enhanced Cardioprotection by Human Endometrium Mesenchymal Stem Cells Driven by Exosomal MicroRNA-21, *Stem Cells Transl Med,* **6**: 209–222. doi:10.5966/sctm.2015-0386.

Wang H, Jin P, Sabatino M, Ren J, Civini S, Bogin V, Ichim TE, Stroncek DF. 2012, Comparison of endometrial regenerative cells and bone marrow stromal cells, *J Transl Med,* **10**: 207. doi:10.1186/1479-5876-10-207.

Webber J, Steadman R, Mason MD, Tabi Z, Clayton A. 2010, Cancer exosomes trigger fibroblast to myofibroblast differentiation, *Cancer Res,* **70**: 9621–9630. doi:10.1158/0008-5472.CAN-10-1722.

Wiśniewski JR, Ostasiewicz P, Mann M. 2011, High recovery FASP applied to the proteomic analysis of microdissected formalin fixed paraffin embedded cancer tissues retrieves known colon cancer markers, *J Proteome Res*, **10**: 3040-3049. doi: 10.1021/pr200019m

Xu C, Yu P, Han X, Du L, Gan J, Wang Y, Shi Y. 2014, TGF-β promotes immune responses in the presence of mesenchymal stem cells, *J Immunol,* **192**: 103–109. doi:10.4049/jimmunol.1302164.

Yoo S-W, Chang D-Y, Lee H-S, Kim G-H, Park J-S, Ryu B-Y, Joe E-H, Lee Y-D, Kim S-S, Suh-Kim H. 2013, Immune following suppression mesenchymal stem cell transplantation in the ischemic brain is mediated by TGF-β, *Neurobiol Dis,* **58**: 249–257. doi:10.1016/j.nbd.2013.06.001.

616   Zhang B, Yin Y, Lai RC, Lim SK. 2014, Immunotherapeutic potential of extracellular

617   vesicles, *Front Immunol,* **5**: 518. doi:10.3389/fimmu.2014.00518.

618

619 **8. Figure legends**

620 **Figure 1. Phenotypic analysis of endMSCs and multipotent differentiation assays.** A)

621 Phenotypic analysis was performed by multicolor flow cytometry. Representative

622 histograms of four different cell lines are shown. The expression level of cell surface

623 markers (CD14, CD20, CD34, CD44, CD45, CD73, CD80, CD90, CD117 and HLA-DR) is

624 represented as Normalized Mean Relative Fluorescence Intensity (MRFI) which is

625 calculated by dividing the Mean Fluorescent Intensity by its isotype control. The MRFI

626 values and the standard deviations obtained from four different cell lines are included in the

627 upper right corner of the histograms. B) Adipogenic, osteogenic and chondrogenic

628 differentiation of endMSCs were induced as described in "Material and Methods". The

629 adipogenic, chondrogenic and osteogenic differentiation degree was quantified by

630 determining the absorbance of the extracts at 490 nm (Oil Red O and Alizarin Red S

631 staining) and at 600 nm (Alcian Blue 8GX). Four independent experiments using four

632 different cell lines were performed and a Mann-Whitney U test was used. C) The *in vitro*

633 differentiations were confirmed by microscopic examination at 20X magnification. The

634 upper images correspond to control cells (non-induced) and lower images to *in vitro*

635 induced differentiations.

636 **Figure 2. Characterization of EV-endMSCs.** A) Representative frequency size

637 distribution graph of EV-endMSCs. The nanoparticle tracking analysis was performed to

638 quantify size distribution and particle concentration (n = 4). B) Flow cytometry expression

639 of CD9 and CD63 in EV-endMSCs-coated latex beads. Representative histograms of CD9

640 and CD63 expression are shown (filled histograms) together with their negative control

641 (gray lined histograms). C) Proteomic characterization of EV-MSCs. A total of 657

642 proteins (with more than two peptides per protein at 1% FDR) were identified in the EV-

643 endMSCs. Among these 657 selected proteins, 480 (75%) were associated to the Gene

644 Ontology term extracellular exosome (GO:0070062, p<<<0.001, 1% FDR) and 62 of them

645 were present in the 100 top identified proteins in Exo Carta database (Keerthikumar *et al.,*

646 2015).

647 **Figure 3. CD45RA and CD62L co-expression on *in vitro* stimulated T cells co-cultured**

648 **in the presence of EV-endMSCs.** At day 6, *in vitro* stimulated PBLs co-cultured with EV-

649 endMSCs at 8, 16 and 32 x10^{10} particles/ml, were analyzed for the co-expression of

650 CD45RA and CD62L. The CD45RA isoform and CD62L distinguished two subsets of T

651 cells: naïve T cells (CD45RA+ CD62L+) and effector memory T cells (CD45RA–CD62L–

652). The peripheral blood lymphocytes from four different healthy donors were co-cultured in

653 the presence of different extracellular vesicles isolated from four different cell lines (n=16).

654 A) percentage of CD4+ naïve T cells, B) percentage of CD4+ effector memory T cells, C)

655 percentage of CD8+ naïve T cells and D) percentage of CD8+ effector memory T cells. The

656 lower boundary of the boxes indicates the 25th percentile and the upper boundary, the 75th

657 percentile. Bars above and below the boxes indicate the 90th and 10th percentiles. The line

32

658 within the boxes marks the median. For variables with normal distribution and

659 homogeneity of variances (CD4+ effector memory T cells and CD8+ effector memory T

660 cells) one-way ANOVA test was performed. When a statistically significant difference was

661 found, a Tukey test was performed to evidence differences between groups. For non-

662 parametric variables (CD4+ naïve T cells and CD8+ naïve T cells), a Kruskal-Wallis test

663 was performed, followed by a Dunn's test when s statistically significant difference was

664 found to evidence differences between groups. *P*-values were considered significant at

665 ≤0.05 (*p≤ 0.05; **p≤ 0.01; ***p≤ 0.001).

666 **Figure 4. Active TGFβ quantification in EV-endMSCs: EV-free fractions and**

667 **ultracentrifuged fractions.** The quantification of active TGFβ was performed by ELISA

668 in different fractions of extracellular vesicle-enriched supernatants from 4 different donors

669 (n=4). The left column represents the amount of active TGFβ in extracellular vesicle-free

670 fractions (normalized on the basis of total protein content). The central column represents

671 the amount of active TGFβ on intact extracellular vesicles purified by ultracentrifugation

672 from EV-endMSCs. The right column represents the amount of active TGFβ on lysed

673 extracellular vesicles. The lower boundary of the boxes indicates the 25th percentile and the

674 upper boundary, the 75th percentile. Bars above and below the boxes indicate the 90th and

675 10th percentiles. The line within the boxes marks the median. The individual values are

676 also shown. Data was analyzed by one-way ANOVA test followed by Tukey test to

677 evidence differences between groups. *P*-values were considered significant at ≤0.05 (**p≤

678 0.01; ****p≤ 0.0001).

679 **Figure 5. TGFβ blockade in *in vitro* stimulated T cells co-cultured with EV-endMSCs**.

680 The *in vitro* stimulation of PBLs was performed for 6 days. These PBLs, obtained from

681 four different donors, were co-cultured with different EV-endMSCs isolated from four

682 different cell lines (n=16) at 8, 16 and 32 x10^{10} particles/ml in the presence or absence of

683 TGFβ-neutralizing antibody at 1μg/ml. The percentages of different T cell subsets from

684 extracellular vesicle-treated PBLs were compared with the appropriate control. The lower

685 boundary of the boxes indicates the 25th percentile and the upper boundary, the 75th

686 percentile. Bars above and below the boxes indicate the 90th and 10th percentiles. The line

687 within the boxes marks the median. The Kruskal-Wallis test for non-parametric data was

688 performed, followed by the Dunn's test when a significant difference was found to

689 evidence differences between extracellular vesicle-treated PBLs and the control without

690 extracellular vesicles. *P*-values were considered significant at ≤0.05 (*p≤0.05; ***p≤0.001;

691 ****p≤0.0001).

692 **Figure 6. Schematic diagram of experimental design and results.** A) *In vitro* stimulation

693 of CD4+ T cells with anti-CD2, anti-CD3 and anti-CD28 that partially mimic the

694 stimulation by antigen-presenting cells. At day 6, the percentage of effector memory CD4+

695 T cells and naïve CD4+ T cells increased and decreased respectively. B) *In vitro*

696 stimulation of CD4+ T cells co-cultured in the presence of EV-endMSCs. At day 6, the

697 differentiation towards effector memory CD4+ T cells was significantly inhibited by EV-

698 endMSCs. C) *In vitro* stimulation of CD4+ T cells co-cultured in the presence of EV-

699 endMSCs blocked with neutralizing TGFβ. Anti-TGFβ partially counteracted the inhibitory

700 effect of extracellular vesicles against *in vitro* activated CD4+ T cells.

701 **Supplementary Figure 1. CD45RA and CD62L co-expression in *in vitro* stimulated T**

702 **cells co-cultured in the presence of extracellular vesicle free-fractions from**

703 **concentrated supernatants.** At day 6, *in vitro* stimulated PBLs co-cultured with

704 extracellular vesicle-free fractions at 20, 40 and 80 μg of total proteins/ml were analyzed

705 for the co-expression of CD45RA and CD62L. The CD45RA isoform and CD62L

706 distinguished two subsets of T cells: naïve T cells (CD45RA+ CD62L+) and effector

707 memory T cells (CD45RA–CD62L–). The peripheral blood lymphocytes were co-cultured

708 in the presence of different extracellular vesicles isolated from four different cell lines

709 (n=4). A) percentage of CD4+ naïve T cells, B) percentage of CD4+ effector memory T

710 cells, C) percentage of CD8+ naïve T cells and D) percentage of CD8+ effector memory T

711 cells. The lower boundary of the boxes indicates the 25th percentile and the upper

712 boundary, the 75th percentile. Bars above and below the boxes indicate the 90th and 10th

713 percentiles. The line within the boxes marks the median. Data were statistically analyzed

714 using the Kruskal-Wallis test, together with the Dunn's test when a statistically significant

715 difference was found, to evidence differences with the CON group. *P*-values were

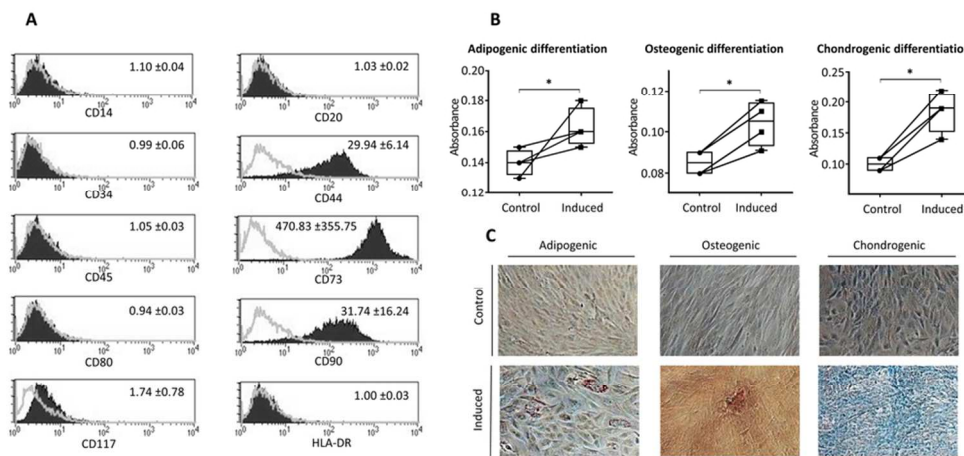716 considered significant at ≤0.05 (*p≤ 0.05; **p≤ 0.01).

Figure 1. Phenotypic analysis of endMSCs and multipotent differentiation assays. A) Phenotypic analysis was performed by multicolor flow cytometry. Representative histograms of four different cell lines are shown. The expression level of cell surface markers (CD14, CD20, CD34, CD44, CD45, CD73, CD80, CD90, CD117 and HLA-DR) is represented as Normalized Mean Relative Fluorescence Intensity (MRFI) which is calculated by dividing the Mean Fluorescent Intensity by its isotype control. The MRFI values and the standard deviations obtained from four different cell lines are included in the upper right corner of the histograms. B) Adipogenic, osteogenic and chondrogenic differentiation of endMSCs were induced as described in "Material and Methods". The adipogenic, chondrogenic and osteogenic differentiation degree was quantified by determining the absorbance of the extracts at 490 nm (Oil Red O and Alizarin Red S staining) and at 600 nm (Alcian Blue 8GX). Four independent experiments using four different cell lines were performed and a Mann-Whitney U test was used. C) The in vitro differentiations were confirmed by microscopic examination at 20X magnification. The upper images correspond to control cells (non-induced) and lower images to in vitro induced differentiations.

87x42mm (300 x 300 DPI)

1
2
3
4
5
6
7
8
9
10
11
12
13
14
15
16
17
18
19
20
21
22
23
24
25
26
27
28
29
30
31
32
33
34
35
36
37
38
39
40
41
42
43
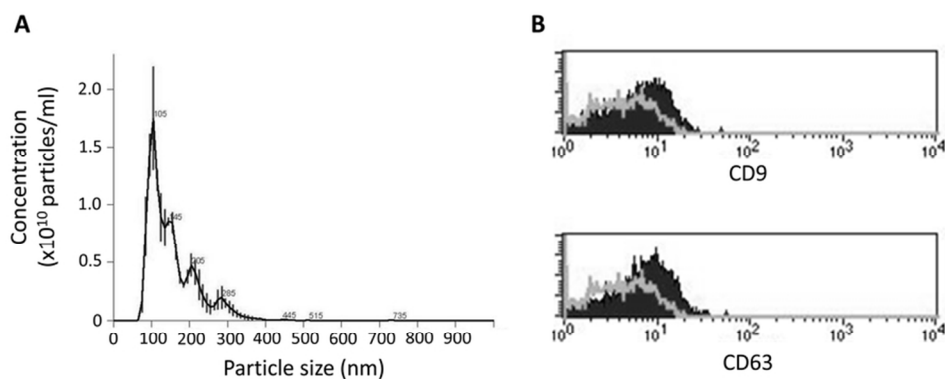44
45
46
47
48
49
50
51
52
53
54
55
56
57
58
59
60

Figure 2. Characterization of EV-endMSCs. A) Representative frequency size distribution graph of EV-endMSCs. The nanoparticle tracking analysis was performed to quantify size distribution and particle concentration (n = 4). B) Flow cytometry expression of CD9 and CD63 in microvesicle-coated latex beads. Representative histograms of CD9 and CD63 expression are shown (filled histograms) together with their negative control (gray lined histograms).
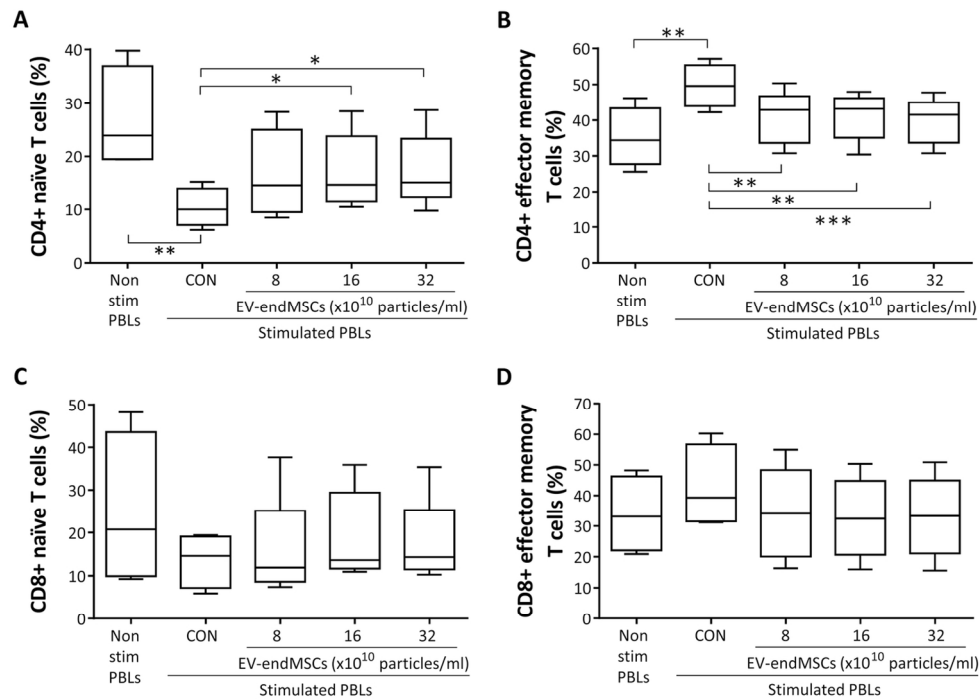
79x35mm (300 x 300 DPI)

Figure 3. CD45RA and CD62L co-expression on in vitro stimulated T cells co-cultured in the presence of EV-endMSCs. At day 6, in vitro stimulated PBLs co-cultured with EV-endMSCs at 8, 16 and 32 $\times 10^{10}$ particles/ml, were analyzed for the co-expression of CD45RA and CD62L. The CD45RA isoform and CD62L distinguished two subsets of T cells: naïve T cells (CD45RA+ CD62L+) and effector memory T cells (CD45RA–CD62L–). The peripheral blood lymphocytes from four different healthy donors were co-cultured in the presence of different extracellular vesicles isolated from four different cell lines (n=16). A) percentage of CD4+ naïve T cells, B) percentage of CD4+ effector memory T cells, C) percentage of CD8+ naïve T cells and D) percentage of CD8+ effector memory T cells. The lower boundary of the boxes indicates the 25th percentile and the upper boundary, the 75th percentile. Bars above and below the boxes indicate the 90th and 10th percentiles. The line within the boxes marks the median. For variables with normal distribution and homogeneity of variances (CD4+ effector memory T cells and CD8+ effector memory T cells) one-way ANOVA test was performed. When a statistically significant difference was found, a Tukey test was performed to evidence differences between groups. For non-parametric variables (CD4+ naïve T cells and CD8+ naïve T cells), a Kruskal-Wallis test was performed, followed by a Dunn's test when s statistically significant difference was found to evidence differences between groups. P-values were considered significant at ≤0.05 (*p≤ 0.05; **p≤ 0.01; ***p≤ 0.001).
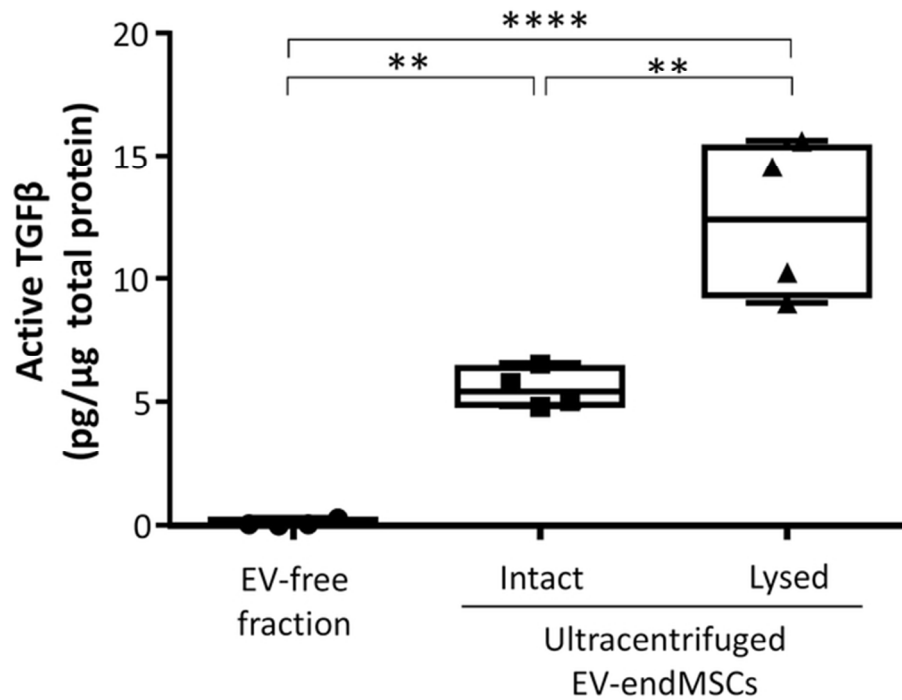
128x92mm (300 x 300 DPI)

Figure 4. Active TGFβ quantification in EV-endMSCs: EV-free fractions and ultracentrifuged fractions. The quantification of active TGFβ was performed by ELISA in different fractions of extracellular vesicle-enriched supernatants from 4 different donors (n=4). The left column represents the amount of active TGFβ in extracellular vesicle-free fractions (normalized on the basis of total protein content). The central column represents the amount of active TGFβ on intact extracellular vesicles purified by ultracentrifugation from EV-endMSCs. The right column represents the amount of active TGFβ on lysed extracellular vesicles. The lower boundary of the boxes indicates the 25th percentile and the upper boundary, the 75th percentile. Bars above and below the boxes indicate the 90th and 10th percentiles. The line within the boxes marks the median. The individual values are also shown. Data was analyzed by one-way ANOVA test followed by Tukey test to evidence differences between groups. P-values were considered significant at ≤0.05 (**p≤ 0.01; ****p≤ 0.0001).
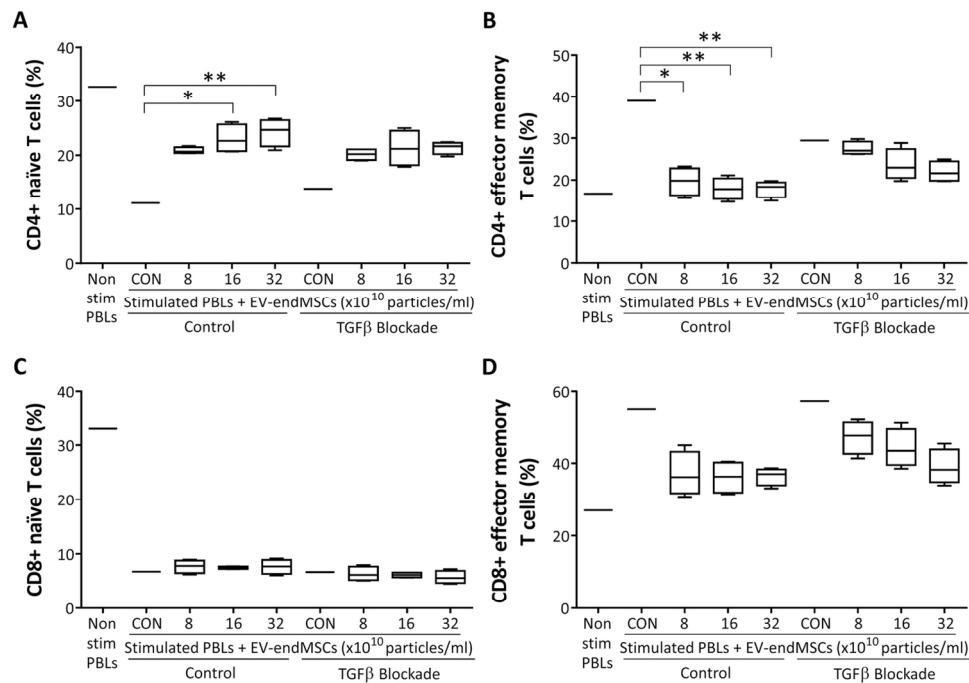
60x46mm (300 x 300 DPI)

Figure 5. TGFβ blockade in in vitro stimulated T cells co-cultured with EV-endMSCs. The in vitro stimulation of PBLs was performed for 6 days. These PBLs were co-cultured with different EV-endMSCs isolated from four different cell lines (n=4) at 8, 16 and 32 x10^{10} particles/ml in the presence or absence of TGFβ-neutralizing antibody at 1 µg/ml. The percentages of different T cell subsets from extracellular vesicle-treated PBLs were compared with the appropriate control. The lower boundary of the boxes indicates the 25th percentile and the upper boundary, the 75th percentile. Bars above and below the boxes indicate the 90th and 10th percentiles. The line within the boxes marks the median. The Kruskal-Wallis test for non-parametric data was performed, followed by the Dunn's test when a significant difference was found to evidence differences between extracellular vesicle-treated PBLs and the control without extracellular vesicles. P-values were considered significant at ≤0.05 (*p≤0.05; **p≤0.01).
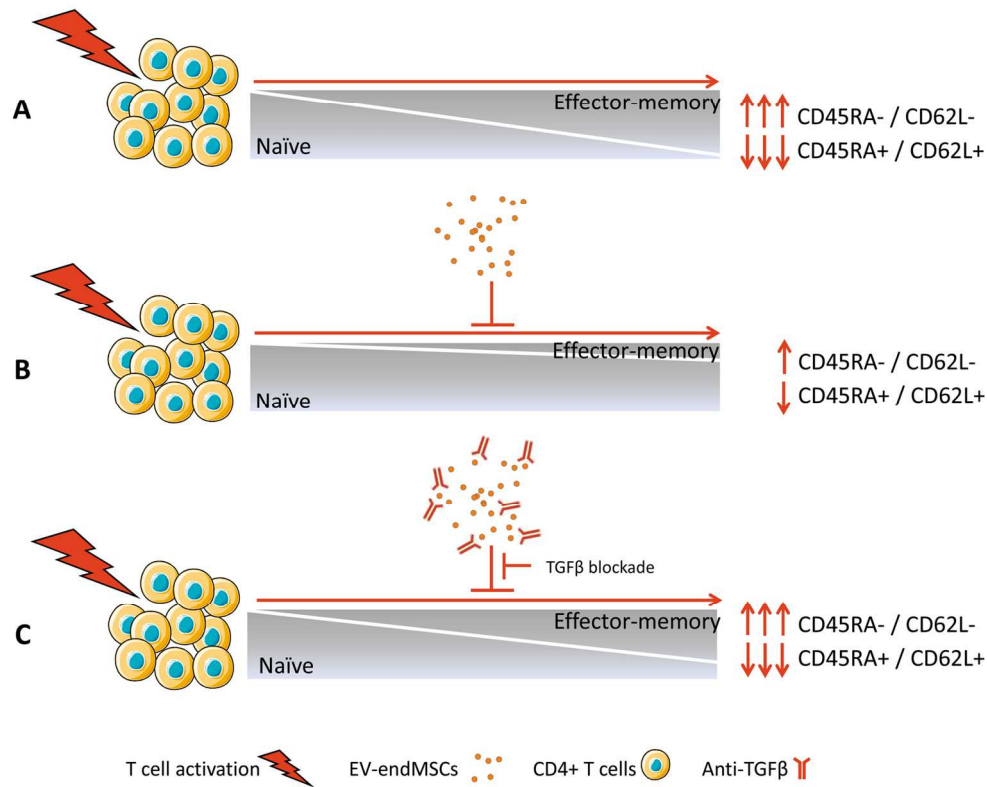
126x89mm (300 x 300 DPI)

Figure 6. Schematic diagram of experimental design and results. A) In vitro stimulation of CD4+ T cells with anti-CD2, anti-CD3 and anti-CD28 that partially mimic the stimulation by antigen-presenting cells. At day 6, the percentage of effector memory CD4+ T cells and naïve CD4+ T cells increased and decreased respectively. B) In vitro stimulation of CD4+ T cells co-cultured in the presence of EV-endMSCs. At day 6, the differentiation towards effector memory CD4+ T cells was significantly inhibited by EV-endMSCs. C) In vitro stimulation of CD4+ T cells co-cultured in the presence of EV-endMSCs blocked with neutralizing TGFβ. Anti-TGFβ partially counteracted the inhibitory effect of extracellular vesicles against in vitro activated CD4+ T cells.

144x115mm (300 x 300 DPI)